Nanoscale Zero-Valent Iron Supported on Graphene Novel Adsorbent for the Removal of Diazo Direct Red 81 from Aqueous Solution: Isotherm, Kinetics, and Thermodynamic Studies

Iran Manesh, Maryam; Sohrabi, Mahmoud Reza*[+]; Mortazavi Nik, Saeed

Department of Chemistry, Islamic Azad University, North Tehran Branch, Tehran, I.R. IRAN

ABSTRACT: *In this study, a nanoscale Zero-Valent Iron-Graphene (nZVI-G) composite was synthesized and applied for the removal of diazo Direct Red 81 from an aqueous solution. The prepared nanocomposite was characterized using Scanning Electron Microscopy (SEM), Energy-Dispersive X-Ray Spectroscopy (EDS), X-Ray Diffraction (XRD)analysis, and Fourier-Transform InfraRred (FT-IR) spectroscopy. The particle size was in the range of 20 to 35 nm. The effect of influential experimental variables on dye removal such as contact time, pH, adsorbent dosage, initial dye concentration, and the temperature was investigated. In optimum conditions, including contact time of 10 min, pH = 3, the adsorbent dosage of 0.05 g, and initial dye concentration=10 mg/L, dye removal was achieved 92%. Different adsorption isotherm models (Langmuir and Freundlich) were used and adsorption followed Langmuir isotherm well (R^2= 0.9773). The maximum Langmuir adsorption capacity of nZVI-G was obtained 29.07 mg/g. The pseudo-first-order kinetic model with R^2=0.9838 fitted well with the experimental data. The thermodynamic parameters ($\Delta G, \Delta H, \Delta S$) were calculated and the results revealed that the adsorption of dye was spontaneous and exothermic. The nZVI-G composite was found to be a low-cost potential candidate with high adsorption capability to be applied as an adsorbent for the removal of Direct Red 81 from the aqueous media. Reduction degradation reaction which rapidly produces radicals has a major effect on reaction time. This nano adsorbent has the ability to adsorb, reduce, and degradation of pollutants, so the dye was removed efficiently.*

KEYWORDS: *Nanoscale zero-valent iron; Graphene; Direct Red 81; Removal; Isotherm; Kinetics.*

INTRODUCTION

Contaminants in the water have become uncontrollable due to the development of various factories. Diverse contaminants such as dyes, heavy metal ions, drugs, and organophosphorus pesticides have a serious influence on the health of aquatic environments and humans [1]. The discharge of sewage, containing dye, which belongs to the textile industries is a serious threat to the environment [2]. Among various types of dyes, half

* *To whom correspondence should be addressed.*
+ *E-mail: sohrabi.m46@yahoo.com*
1021-9986/2022/6/1844-1855 12/$/6.02

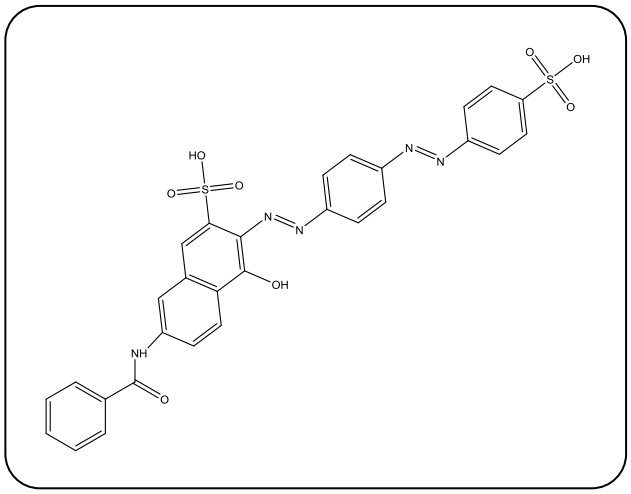

Scheme 1: Chemical structure of Direct Red 18.

of the whole dyes used in the textile industry are Azo dyes. −N=N− is the usual structure of these dyes and carbon bonding on both sides of them is with sp^2 hybrid [3]. These dyes have high stability versus physical, chemical, and biological factors due to their complex aromatic structure, which leads to the impossibility of destruction [4]. One of the sulfonated Azo dyes is Direct Red 81 with the chemical name of disodium (3E)-7-benzamido-4-oxo-3-[[4-[(4-sulfonatophenyl)diazenyl] phenyl] hydrazinylidene] naphthalene-2-sulfonate (Scheme 1). Carcinogenic properties and toxicity of this dye can affect humans, animals, and plants [5,6]. Therefore, preventing the discharge of synthetic dyes from industrial wastewater into the environment is the most important issue. Different ways for removing dyes have been reported such as ozonation [7], oxidation [8], coagulation [9], electrocoagulation/flotation [10], coagulation/flocculation [11], electrochemical [12], and adsorption [13]. Among the aforementioned, the adsorption procedure has been further recommended owing to its sludge-free, flexibility, simplicity of operation, and low-cost [14-16].

Many adsorbents including activated carbon [17], chitosan [18], zero-valent iron nanoparticles [19], graphene oxide aerogel [20], magnesium oxide nanoparticles loaded onto activated carbon [21], magnesium oxide nanoparticles immobilized with chitosan [22], etc. have been assessed to remove dye by investigators. High reactivity and large surface area are known as advantages of nanoscale zero-valent iron (nZVI) particles, which has caused its widespread use. Oxidation of nZVI into Fe^{2+} or Fe^{3+} can occur and donate electrons, which leads to adsorbing heavy metals, dyes, and so on. Also, nZVI is known as a strong reducing agent and provides a suitable reductive environment for the growth of anaerobic microorganisms [23,24]. Due to the reduction degradation reaction of Fe° which rapidly produces radicals, the reaction time will be reduced. However, high van der Waals and magnetic attraction forces of nZVI lead to aggregation. Therefore, by reducing the reactivity surface area, the efficiency of pollutant removal decreases [23,25]. Reducing the agglomeration of nZVI particles with supporting materials on the substrate has been reported by researchers. Furthermore, improved dispersal ability and specific surface area, as well as increasing its reactivity are observed [26,27]. Iron is a compound that is found in high amounts in nature and it is environmentally compatible and low-cost. Recently, some materials like zeolite [28], bentonite [29], chitosan [30], and graphene [31] were applied to support nZVI particles. These materials can prevent oxidation and aggregation *by* providing steady sites for nZVI particle loading because of their excellent surface area and porous structure [27].

Graphene (G) has been taken into consideration as a superior supporter material for loading nanoparticles due to its large surface area, high flexibility, 2D substrates, pore volumes, and excellent conductivity despite its time-consuming synthesis process [32,33]. Recently, a combination of nZVI and graphene is a topic that has received special attention. Their combination represents a remarkable increase in their efficiency through their adsorption and reduction of degradation features.

nZVI alone or along with the other materials have been used to remove different dyes from aqueous environments in previous research. According to the literature, removal efficiency has been increased by coupling nZVI with other materials. There were no reports about nZVI coupled with graphene for the removal of Direct Red 81. Hence, in this study, nZVI-G composite was synthesized to remove Direct Red 81 dye from aqueous media. The synthesized composite was characterized using a Scanning Electron Microscope (SEM), Energy-Dispersive X-ray Spectroscopy (EDS), X-Ray Diffraction (XRD) analysis, and Fourier-Transform InfraRed (FT-IR) spectroscopy. The effective experimental parameters on the removal performance, including the contact time, pH, the adsorbent dosage, and pollutant concentration were optimized. Finally, isotherms and kinetics models, as well as thermodynamic parameters were investigated.

EXPERIMENTAL SECTION

Materials

Graphite, Sodium nitrate ($NaNO_3$), Sulfuric acid (H_2SO_4), Potassium permanganate ($KMnO_4$), Hydrogen peroxide (H_2O_2), sodium borohydride ($NaBH_4$), and iron (III) chloride hexahydrate ($FeCl_3{\cdot}6H_2O$) were purchased from Merck. Direct Red 81 was provided by AlvanSabet Co., in an industrial purity. Distilled water was used as the solvent.

Apparatus

The morphology of the synthesized nanocomposite was observed by the ZEISS SEM (SIGMA VP, Germany). The elemental analysis was performed using EDS (Oxford Instruments, England). For EDS analysis, the sample should be an electrical conductor, so its surface is coated before testing. This coating usually consists of gold (Au), and the presence of Au in the EDS spectrum is due to this coverage. XRD analysis of nZVI-G with a Cu-Kα radiation source was studied by a Panalytical X-ray diffractometer. The infrared spectrum of the adsorbent was obtained by PerkinElmer FT-IR. Philler scientific double beam UV-Vis spectrophotometer (SU-6100, Belgium) was used for spectrophotometric measurements. Metrohm pH meter (model 691, Switzerland) was utilized to adjust the pH values.

Preparation of graphene

Hummers' method was used for graphene synthesis. At first, 120 mL H_2SO_4 was placed in the ice bath for 5 min to reduce its temperature. Then, 5 g graphite plus 2.5 g of $NaNO_3$ was added while stirring. 15 g of $KMnO_4$ was gradually added for 20 min. The obtained solution was kept at room temperature for about 30 min. Afterward, 230 mL of distilled water was added and the temperature was increased to 95 °C. Again 700 mL of distilled water and 10 mL of H_2O_2 were added to obtain a yellow mixture. Graphene oxide (GO) was obtained by washing and filtering the mixture. To prepare graphene, H_4BNa was added gradually as a reducing agent for 30 min. The obtained precipitate was graphene, which was washed with water and ethanol mixture 3 times, as well as with distilled water for the last time, and placed in the oven at 50-60 °C for 24 h [34].

Preparation of nano zero-valent iron/graphene composite

200 mL of distilled water was deoxygenated for 5 min under mechanical stirring with nitrogen gas. Then, 2 g $FeCl_3{\cdot}6H_2O$ was added. After 5 min, 0.3 g of graphene was added and the mixture was stirred for 10 to 15 min along with nitrogen gas using a mechanical stirrer. During this period, 1 g $NaBH_4$ was dissolved in distilled water and was made to the mark in the 100 mL volumetric flask. After 10-15 minutes, this solution was added dropwise to the mixture using a burette. The mixture was finally stirred for 15 min under nitrogen gas and filtered with a vacuum pump. The obtained precipitate oxidizes rapidly, so it was kept in acetone [35].

Adsorption experiments

Different experimental parameters such as contact time (2−10 min), pH (3-8), adsorbent dosage (0.02−0.1 g/L), initial concentration (5−15 mg/L), and temperature (288−308 K) were investigated. The dye solution was prepared at specific concentrations and a certain amount of nano adsorbent was added, then stirred at the specified temperature, pH, and time. Finally, the residual concentration of dye was determined by spectrophotometry at the wavelength (λ_{max} = 512 nm). The Direct Red 81 removal percentage was calculated as follows:

$$\text{Removal}(\%) = \frac{C_0 - C_e}{C_0} \times 100 \quad (1)$$

Herein, C_0 (mg/L) and C_t (mg/L) represent the initial and the final concentration of the dye in the solution, respectively [36].

RESULTS AND DISCUSSION

Characterization

The XRD pattern of graphene is demonstrated in Fig. 1(a), which corresponds to the reference sample patterns. In this Fig, the peak at the position of 20º shows the graphene index for the plane (002), which is related to the C=C. The peak equal to 47º and 54º is related to the (101) and (004), respectively. The peak observed at 2θ value equal to 54.23° is related to the (004) plane. According to the XRD of the nanocomposite (Fig. 1b), zero-valent iron nanoparticles are immobilized by graphene. These connections are physical and have no effect on the graphene structure. Peaks of 43.3° and 62.8º could be indexed to the (110) and (200) planes of Fe^0 (JCPDS 65-4899), respectively. Small peaks related to Fe_3O_4 are visible at 35.7°, which is the result of oxidation by O_2 in water or air during the process of nZVI preparation and preservation. [33,37].

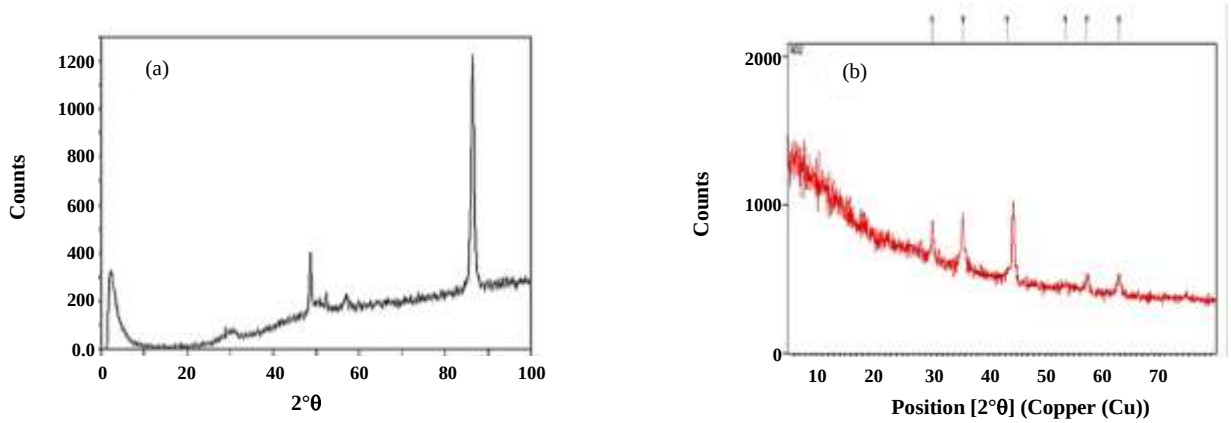

Fig. 1: XRD pattern of (a) graphene and (b) nZVI-G composite.

Figs. 2(a) and (b) show the SEM images of the synthesized nanocomposites at 2 different magnifications. Zero iron particles were uniformly dispersed in the graphene substrate. As can be seen, the graphene was surrounded by iron nanoparticles and covered them. Besides its uniformity by placing nZVI in the graphene substrate, the oxygen access to Fe^{o} was declined so it was increased its stability. Fig. 2 (c) shows the porous structure of graphene, which is a proper place for nZVI particles. The particle size is in the range of 20 to 35 nm.

As shown in the EDS spectrum of the nZVI-G (Fig. 3), the peaks corresponding to Fe are visible in the energy ranges of 0.7, 6.4, and 7.1 keV. In addition, O and C peaks are observed in the 0.5 and 0.3 keV ranges, respectively. The figure shows that the percentages of Fe, O, and C nanoparticles related to the nZVI-G were 50.2, 35.8, and 14, respectively. The presence of iron indicates the composite formation [37,38].

In order to confirm the main functionalities on the nZVI-G, FTIR spectral analysis was performed in the range of 400−4000 cm^{-1} as shown in Fig. 4. The OH group appeared at 3422 cm^{-1} due to the presence of water molecules in the nanocomposite structure. The sharp peak at 1631 cm^{-1} corresponds to the C=C stretching. Moreover, the presence of a peak at 1389 cm^{-1} was assigned to asymmetric stretching vibrations of −COO group. The peak at 613 cm^{-1} is related to the stretching vibration of Fe−O in the structure of Fe_3O_4 magnetic nanoparticles [39,40].

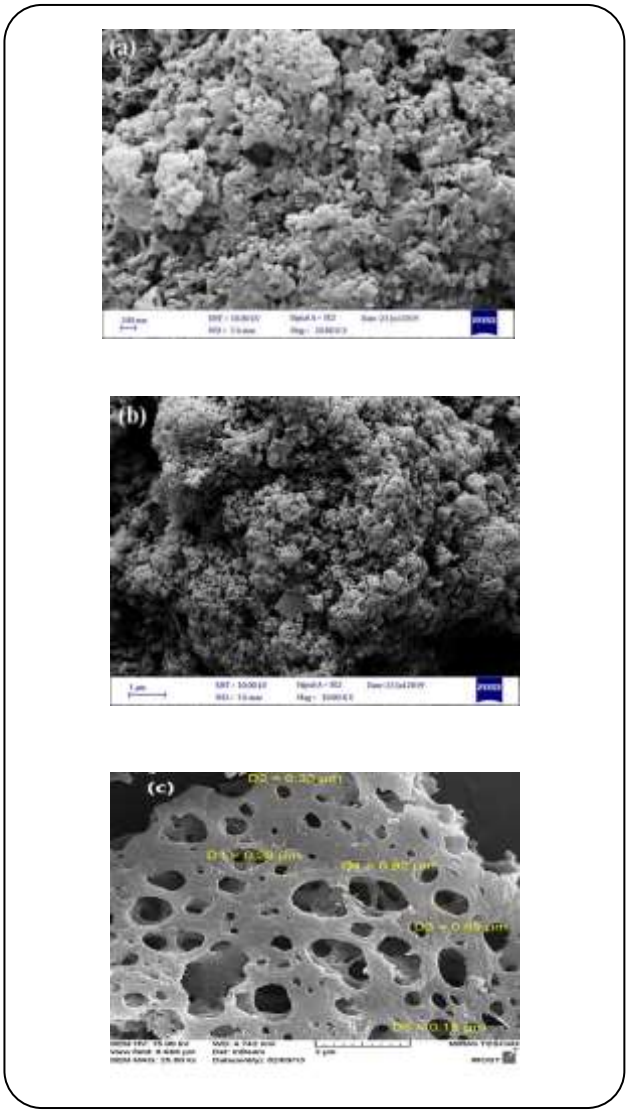

Fig. 2: SEM image of nZVI-G with the magnification of (a) 200 nm and (b) 1 µm and (c) SEM image of graphene with the magnification of 2 µm.

Optimization of adsorption parameters

Effect of pH

pH is one of the most important and effective parameters in controlling the adsorption process.

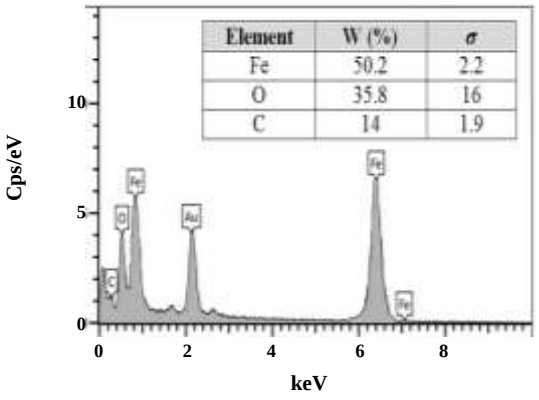

Fig. 3: EDS spectrum of nZVI-G composite.

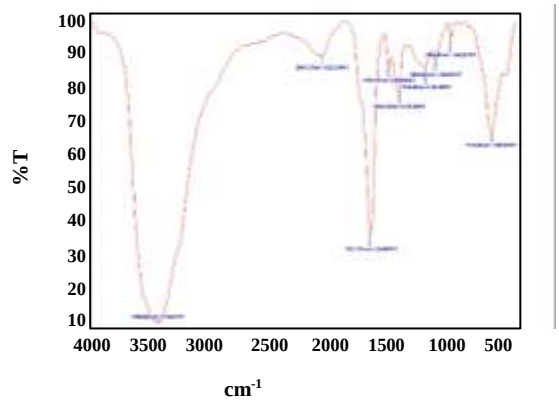

Fig. 4: FT-IR spectrum of nZVI-G.

The effect of different pHs on dye removal efficiency at times of 2, 4, 6, 8, and 10 min is illustrated in Fig. 5 (a). The results included that pH=3 at a time of 10 min had the highest percentage of dye removal. At low pH, hydrogen ions surround the adsorbent surface, where simple electrostatic attraction occurs between the positively charged adsorbent surface and the dye molecules. On the other hand, there is a negatively charged adsorbent surface at higher pH, which decreases the adsorption of dye molecules [5,41]. In an acidic pH, hydrogen was adsorbed to the surface and the rate of hydrogen radical production was increased. So, the reduction degradation process becomes more efficient [42].

$$Fe^{\circ} \leftrightarrow Fe^{2+} + 2e^{-} \quad (2)$$

$$2H^{+} + 2e^{-} \leftrightarrow 2H_{ads} \quad (3)$$

$$nH_{ads} \leftrightarrow nH^{+} + ne^{-} \quad (4)$$

$$Dye(Ox.state) + ne^{-} \leftrightarrow dye(Red.state) \quad (5)$$

Below the pH_{zpc}, the adsorbent is positive in terms of electrostatically (Fig. 5 b).

Effect of adsorbent dosage

The adsorbent dosage of 0.02, 0.05, and 0.1 g was evaluated for 2 to 10 min. The results are shown in Fig. 5 (c). At high doses of the adsorbent, the number of active sites of adsorption increases and leads to enhance dye removal efficiency. It can be concluded that the optimal dosage of adsorbent with a maximum adsorption capacity (92%) was 0.05 g. As can be seen in Fig. 5(c), there are no significant differences between 0.05 and 0.1 g, so 0.05 g of the adsorbent is more admissible. The use of high doses of the adsorbent leads to accumulation, which makes smaller adsorbent particles adhere together, thereby reducing the effective surface area and the number of active adsorption sites, which in turn diminishes dye removal efficiency.

Effect of dye concentration

The concentrations between 5 to 15 mg/L at 2 to 10 min were used to determine the optimum initial dye concentration. As shown in Fig. 5 (d), the maximum removal efficiency belongs to the initial concentration of 10 mg/L. There are many empty sites on the surface of the adsorbent at low concentrations, and many molecules are adsorbed by the nanocomposite and the removal efficiency increased. By increasing the initial dye concentration up to 15 mg/L, the occupation of these adsorption sites has occurred with the dye molecules, the adsorption of the remaining molecules has become more difficult and adsorption decreased.

Effect of temperature

The dye removal efficiency was investigated at 3 different temperatures (288, 298, 308 K) and a constant time of 10 min (Fig. 5 e). The temperature of 308 K with a concentration of 15 mg/L showed the highest value of dye removal. By increasing the temperature, the process rate was enhanced.

Adsorption isotherm models

Langmuir and Freundlich adsorption isotherm models as a powerful tools were used to determine the relationship between the adsorbate concentration and adsorbent. Langmuir equation can be represented as:

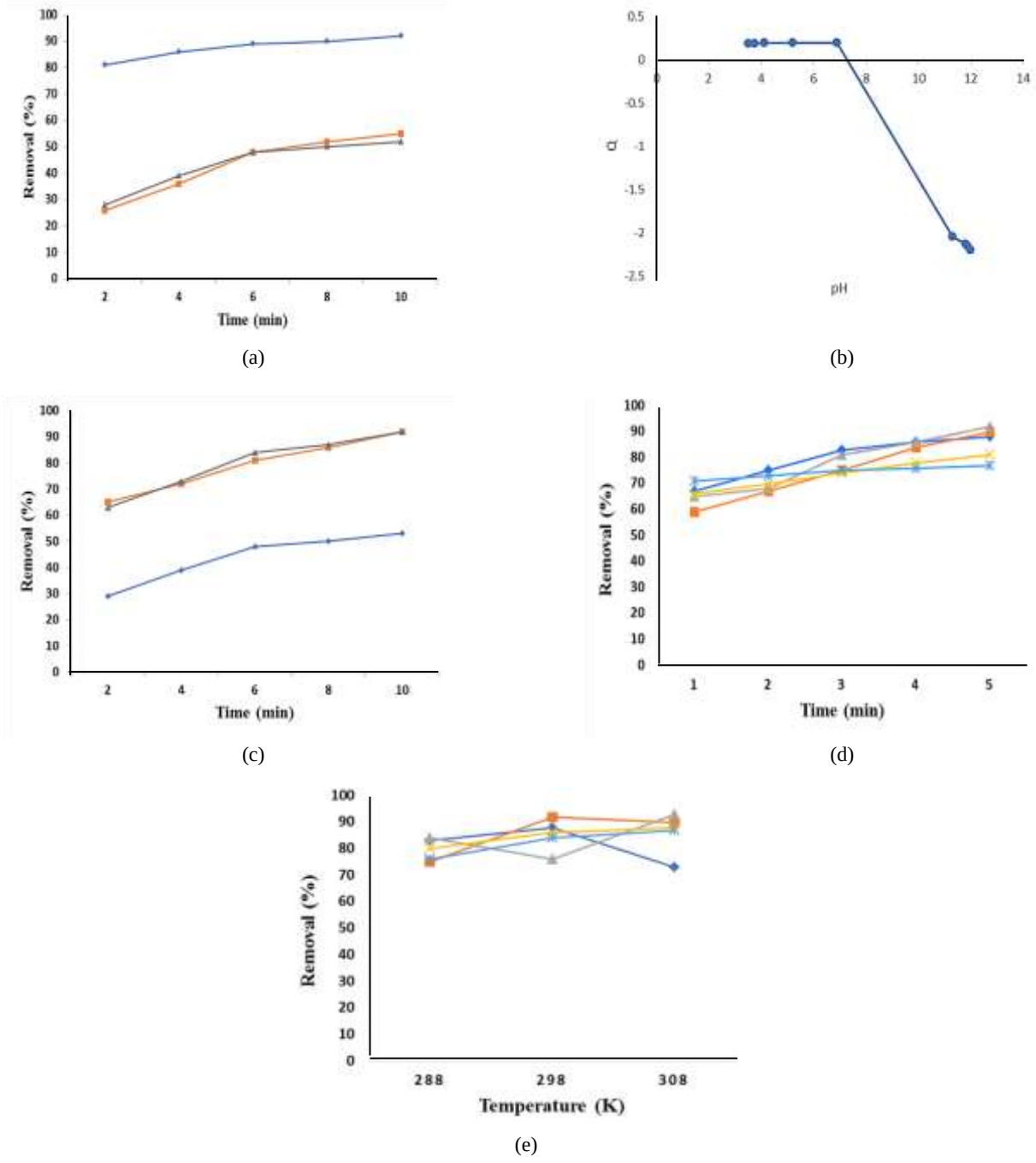

Fig. 5: The effect of (a) pH, (b) pH_{zpc}, (c) adsorbent dosage, (d) initial concentration, and (e) the temperature on dye removal percentage.

$$\frac{1}{q_e} = \frac{1}{q_m} + \frac{1}{K_l q_m}\frac{1}{C_e} \quad (6)$$

Herein q_e (mg/g) and q_m (mg/g) are the amount of dye adsorbed at equilibrium and the maximum adsorption capacity, respectively. C_e (mg/L) shows the dye concentration at equilibrium and K (L/mg) is Langmuir's adsorption constant corresponding to the energy of adsorption. By plotting $1/q_e$ versus $1/Ce$ (Fig. 6 a), the q_m and K_L can be calculated from the intercept and slope of the straight line, respectively [43,44].

The Freundlich isotherm is defined using Eq (7).

Table 1: The obtained parameters of isotherm models for dye removal.

Langmuir			Freundlich		
q_{max} (mg/g)	K_L (l/mg)	R^2	K_f	n	R^2
29.07	2.22	0.9773	26.32	1.46	0.9537

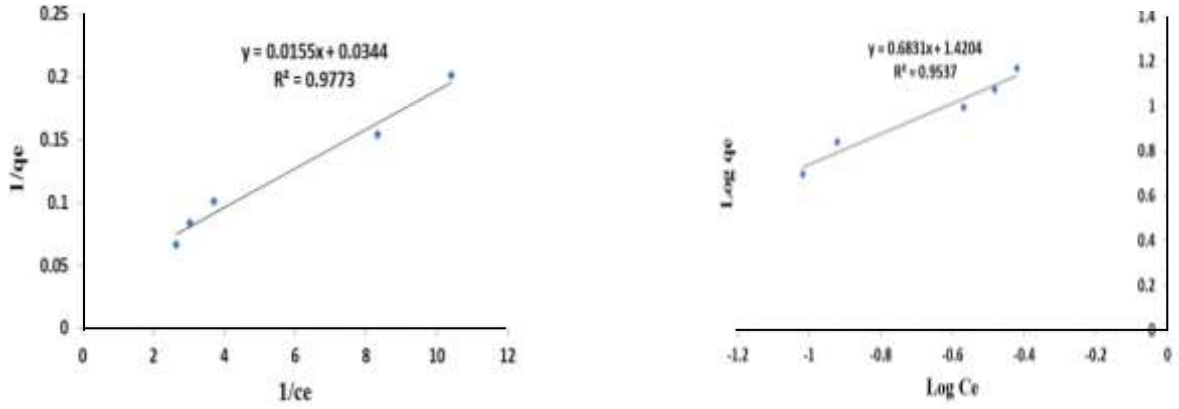

Fig. 6: Langmuir and (b) Freundlich models for the adsorption of dye by nZVI-G composite.

$$\log q_e = \log k_f + \frac{1}{n}\log C_e \quad (7)$$

Where k_f and n indicate the adsorption capacity and adsorption intensity, respectively. These parameters can be calculated by plotting the log q_e against log C_e (Fig. 6 b) [45].

As shown in Fig. 6 (a) and (b), the coefficient of determination (R^2) related to the Langmuir is higher than the Freundlich, which indicated that the adsorption of dye fitted to this model. It can be concluded that the adsorption process of Direct Red 81 is the monolayer. The isotherm parameters are listed in Table 1.

Adsorption kinetics

In this study, with respect to time, the pseudo-first-order and pseudo-second-order kinetic models were investigated to determine the exchanges in dye molecule adsorption. The pseudo-first-order kinetic model is expressed by equation (8).

$$\ln(q_e - q_t) = \ln(q_e) - K_1 t \quad (8)$$

Herein q_e and q_t (mg/g) represent the amount of dye adsorbed on the adsorbent at equilibrium and time t, respectively. K_1 (min^{-1}) shows the rate constant at equilibrium. By plotting linear ln $(q_e - q_t)$ versus time, the rate constant, slope, and intercept can be calculated [46,47].

The pseudo-second-order kinetic model can be represented by the Equation (9).

$$\frac{t}{q_t} = \frac{1}{K_2 q_e^2} + \frac{t}{q_e} \quad (9)$$

Where the rate constant of pseudo-second-order kinetic is shown by K_2 (g/mg min^{-1}). The slope and intercept related to the plot of t/q_t versus t are considered to calculate the K_2 and q_e, respectively [48]. As shown in Fig. 7 (a) and (b), the coefficient of determination (R^2) (0.9838) related to the pseudo-first-order is better than the pseudo-second-order, which indicated that the adsorption of dye fitted to this model. The obtained kinetic parameters for the adsorption of dye are given in Table 2.

Thermodynamic parameters

Standard free energy change (ΔG°) (kJ/mol), standard enthalpy change (ΔH°) (kJ/mol), and the standard entropy change (ΔS°) (kJ/mol.K) as thermodynamic parameters were evaluated using the following equations:

$$\ln K_c = \frac{\Delta S^\circ}{R} - \frac{\Delta H^\circ}{RT} \quad (10)$$

$$\Delta G = \Delta H^\circ - T\Delta S^\circ \quad (11)$$

Table 2: The obtained kinetic parameters for Direct Red 81 removal.

pseudo-first order			Pseudo-second order		
K_1 (min^{-1})	q_e (mg/g)	R^2	K_2 ($g.mg^{-1}. min^{-1}$)	q_e (mg/g)	R^2
0.6047	6.12	0.9838	0.97	11.74	0.9746

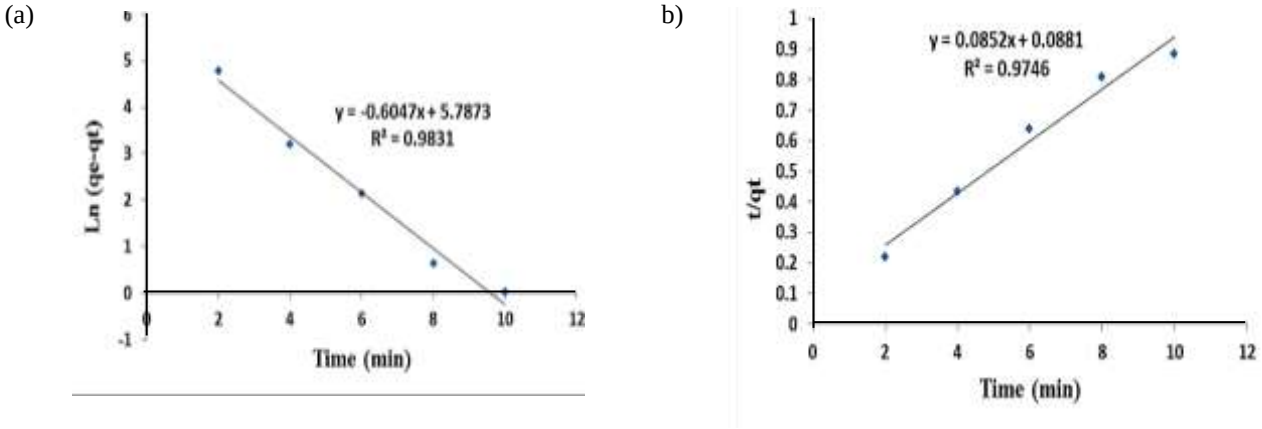

Fig. 7: (a) pseudo-first-order and (b) pseudo-second-order kinetics for the removal dye.

Herein *T*, *R*, and K_c are the absolute temperature (K), the universal gas constant (8.314 J/(mol.K)), and adsorption distribution coefficient, respectively [49,50].

According to Vant Hoff's equation, Ln k versus 1/T was plotted (Fig 8). Also, the results of thermodynamic data for the adsorption of Direct Red 81 onto the nZVI-G composite are summarized in Table 3. The negative value of ΔG indicates the spontaneous reaction of Direct Red 81 adsorption onto nZVI-G. The negative values of ΔH and ΔS demonstrated that the adsorption of this dye was exothermic.

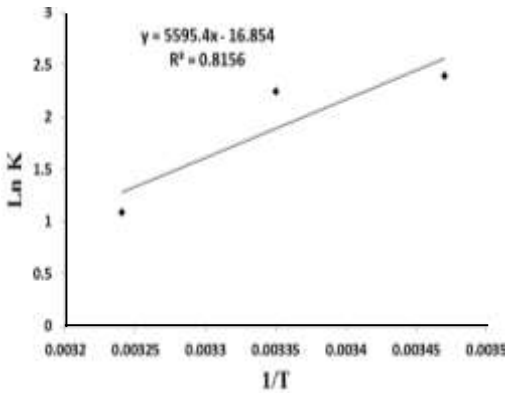

Fig. 8: LnK versus 1/T for Direct Red 81 removal.

Comparison with the other adsorbents

The adsorption capacity of Direct Red 81 on nZVI-G composite as an adsorbent compared with some other adsorbents is shown in Table 4. As can be seen, the adsorption capacity of this dye using nZVI-G is higher than the mentioned adsorbents in less time. Reduction degradation reactions that rapidly produce hydrogen radicals are the major reason for their short reaction times. The reaction time is also very short compared to other adsorbents. Hence, the synthesized adsorbent in the present study showed a high capacity for the removal of Direct Red 81 from aqueous media.

CONCLUSIONS

The novel rapid and efficient nZVI-G composite was successfully prepared using the facile method for the removal of Direct Red 81 dye. The reduction degradation property of nZVI was increased by graphene as a supporter material. The obtained nanocomposite exhibited a high dye removal percentage (>92%). Both components are environmentally compatible and their combination helps increase higher efficiency of the adsorbent due to their adsorption and reduction degradation features. The experimental variables were optimized and the results

Table 3: Thermodynamic parameters for removal of Direct Red 81.

ΔH^0 (kJ/mol)	ΔS^0 (J/ mol K)	ΔG^0 (kJ/mol)		
-46.5	-140	Temperature (K)		
		288	298	308
		-5.7	-5.5	-2.8

Table 4: Comparison of nZVI-G adsorbent with the other adsorbents.

Adsorbent	Adsorption capacity (mg/g)	References	Time (min)	Dye
NaOH-modified rice husk Pumice	14.77	[6]	---	Direct Red 81
Pumice	1.83	[51]	120	Direct Red 81
Neutral soil containing copper	41.84	[52]	60	Direct Red 81
Treated bamboo sawdust	13.83	[53]	60	Direct Red 81
Nano-scale zero-valent iron-Graphene	29.07	This study	10	Direct Red 81

indicated that the removal of this dye increased with increasing adsorbent dosage. It was found that the maximum removal and reduction degradation happened at acidic pH. Also, the removal efficiency was increased with the increasing initial concentration up to 15 mg/L. The study of R^2 of Langmuir and Freundlich isotherm models represented that the adsorption data fitted well with the Langmuir model. The pseudo-first-order kinetic model was appropriate for the adsorption of the mentioned dye. The calculated thermodynamic parameters indicated that the Direct Red 81 adsorption on nZVI-G is a spontaneous and exothermic process. The proposed adsorbent can be a promising solution for dye removal from aqueous solutions.

Received : May 29, 2021 ; Accepted : Aug. 2, 2021

REFERENCES

[1] Ren J., Chul Woo Y., Yao M., Lim S., Tijing L.D., Kyong Sh., Nanoscale Zero-Valent Iron (nZVI) Immobilization onto Graphene Oxide (GO)-Incorporated Electrospun Polyvinylidene Fluoride (PVDF) Nanofiber Membrane for Groundwater Remediation via Gravity-Driven Membrane Filtration, *Science of the Total Environment.*, **688**: 787-796 (2019).

[2] Shojaei S., Shojaei S., Sasani M., The Efficiency of Eliminating Direct Red 81 by Zero- Valent Iron Nanoparticles from Aqueous Solutions Using Response Surface Model (RSM), *Modeling Earth Systems and Environment.*, **3**: 27- (2017).

[3] Sohrabi M.R., Amiri S., Fard Masoumi H.R., Moghri M., Optimization of Direct Yellow 12 Dye Removal by Nanoscale Zero-Valent Iron Using Response Surface Methodology, *Journal of Industrial and Engineering Chemistry*, **20**: 2535-2542 (2014).

[4] Guardão Franca R.D., Vieira A., Carvalho G., Oehmen A., Pinheiro H.M., Barreto Crespo M.T., Lourenco N.D., Oerskovia Paurometabola Can Efficiently Decolorize Azo Dye Acid Red 14 and Remove its Recalcitrant Metabolite, *Ecotoxicology and Environmental Safety*, **191**:110007 (2020).

[5] Khamparia Sh., Jaspal D., Adsorptive Removal of Direct Red 81 Dye from Aqueous Solution onto Argemone Mexicana, *Sustainable Environment Research*, **26**: 117-123 (2016).

[6] Ashrafi S.D., Kamani H., Mahvi A.H., The Optimization Study of Direct Red 81 and Methylene Blue Adsorption on NaOH-Modified Rice Husk, Desalination and Water Treatment., **57**: 738-746 (2016).

[7] Gharbani P., Tabatabaii S.M., Mehrizad A., Removal of Congo Red from Textile Wastewater by Ozonation, *International Journal of Environmental Science & Technology*, **5**: 495-500 (2008).

[8] Atalay S., Ersoz G., Advanced Oxidation Processes for Removal of Dyes from Aqueous Media, Green Chemistry for Dyes Removal from Wastewater: Research Trends and Applications, *Chapter*, **3**: 83-117 (2015).

[9] Shi B., Li G., Wang D., Feng C., Tang H., Removal of Direct Dyes by Coagulation: The Performance of Preformed Polymeric Aluminum Species, *Journal of Hazardous Materials.*, **143**: 567-574 (2007).

[10] Zodi S., Merzouk B., Potier O., Lapicque F., Leclerc J.P., Direct Red 81 Dye Removal by a Continuous Flow Electrocoagulation/Flotation Reactor, *Separation and Purification Technology*, **108**: 215-222, (2013).

[11] Sadri Moghaddam S., Alavi Moghaddam M.R., Arami M., Coagulation/Flocculation Process for Dye Removal Using Sludge from Water Treatment Plant: Optimization Through Response Surface Methodology, *Journal of Hazardous Materials*, **175**: 651-657 (2010).

[12] Gercel O., Removal of Textile Dye from Aqueous Solution by Electrochemical Method, *Journal Separation Science and Technology.*, **51**: 711-717 (2016).

[13] Senthilkumar R., Reddy Prasad D.M., Govindarajan L., Saravanakumar K., Naveen Prasad B.S., Improved Sorption of Reactive Black 5 by Date Seed-Derived Biochar: Isotherm, Kinetic, and Thermodynamic Studies, *Separation Science and Technology*, **54**: 2351-2360 (2019).

[14] Delnavaz, M., & Kazemimofrad, Z., Nano Zerovalent Iron (NZVI) Adsorption Performance on Acidic Dye 36 Removal: Optimization of Effective Factors, Isotherm and Kinetic Study, *Environmental Progress & Sustainable Energy*, 1-13 (2019).

[15] Pourabadeh A., Baharinikoo L., Shojaei S., Mehdizadeh B., Davoodabadi Farahani M., Shojaei S., Experimental Design and Modelling of Removal of Dyes Using Nano-Zero-Valent Iron: A Simultaneous Model, *International Journal of Environmental Analytical Chemistry*, **100**: 1707-1719 (2019).

[16] Saravanakumar K., Senthilkumar R., Reddy Prasad D.M., Naveen Prasad B.S., Manickam S., Gajendiran V., Batch and Column Arsenate Sorption Using *Turbinaria ornata* Seaweed Derived Biochar: Experimental Studies and Mathematical Modeling, *ChemistrySelect*., **5**: 3661 –3668 (2020).

[17] Shu Hui T., Ahmad Zaini M.A., Development of Activated Carbon Pellets Using a Facile Low-Cost Binder for Effective Malachite Green Dye Removal, *Journal of Cleaner Production*, **253**: 119970 (2020).

[18] Pietrelli L., Francolini I., Piozzi A., Dyes Adsorption from Aqueous Solutions by Chitosan, *Separation Science and Technology*, **50**: 1101-1107 (2015).

[19] Hamdy A., Mostafa M.K., Nasr M., Zero-Valent Iron Nanoparticles for Methylene Blue Removal from Aqueous Solutions and Textile Wastewater Treatment, with Cost Estimation, *Water Science & Technology*, **78**: 367-378 (2018).

[20] Hoang Tu T., Thi Ngoc Cam P., Van Trong Huy L., Thanh Phong M., Minh Nam H., Huu Hieu N., Synthesis and Application of Graphene Oxide Aerogel as an Adsorbent for Removal of Dyes from Water, *Materials Letters*, **238**: 134-137 (2019).

[21] Myneni V.R., Punugoti T., Kala N.S., Kanidarapu N.R., Vangalapati M., Modelling and Optimization of Methylene Blue Adsorption onto Magnesium Oxide Nanoparticles loaded onto Activated Carbon (MgONP-AC): Response Surface Methodology and Artificial Neural Networks, *Materials Today: Proceedings*, **18:** 4932–4941 (2019).

[22] Myneni V.R., Kanidarapu N.R., Vangalapati M., Methylene Blue Adsorption by Magnesium Oxide Nanoparticles Immobilized with Chitosan (CS-MgONP): Response Surface Methodology, Isotherm, Kinetics and Thermodynamic Studies, *Iran. J. Chem. Chem. Eng. (IJCCE)*, **39 (6)**: 29-42 (2020).

[23] Mehrabi N., Masud A., Afolabi M., Hwang J., Calderon Ortizc G.A., Aich N., Magnetic Graphene Oxide-Nano Zero Valent Iron (GO–nZVI) Nanohybrids Synthesized Using Biocompatible Cross-Linkers for Methylene Blue Removal, *RSC Advances*, **9**: 963-973 (2019).

[24] Erdima E., Yucesoy Ozkan Z., Kurt H., Alpaslan Kocamemi B., Overcoming Challenges in Mainstream Anammox Applications: Utilization of Nanoscale Zero Valent Iron (nZVI), *Science of the Total Environment*., **651**: 3023-3033 (2019).

[25] Li J., Chen C., Zhu K., Wang X., Nano Scale Zero-Valent Iron Particles Modified on Reduced Graphene Oxides Using a Plasma Technique for Cd (II) Removal, *Journal of the Taiwan Institute of Chemical Engineers*, **59**: 389-394 (2016).

[26] Zheng T., Zhan J., He J., Day C., Lu Y., McPherson G.L., Piringer G., John V.T., Reactivity Characteristics of Nanoscale Zerovalent Iron−Silica Composites for Trichloroethylene Remediation, *Reactivity Environmental Science & Technology*, **42**: 4494-4499 (2008).

[27] Lv X., Xu J., Jiang G., Xu X., Removal of Chromium (VI) from Wastewater by Nanoscale Zero-Valent Iron Particles Supported on Multiwalled Carbon Nanotubes, *Chemosphere*, **85**: 1204-1209 (2011).

[28] Suazo-Hernandez J., Sepulveda P., Manquian-Cerda K., Ramírez-Tagle R., Angélica Rubio M., Bolan N., Sarkar B., Arancibia-Miranda N., Synthesis and Characterization of Zeolite-Based Composites Functionalized with Nanoscale Zero-Valent Iron for Removing Arsenic in the Presence of Selenium from Water, *Journal of Hazardous Materials*, **373**: 810-819 (2019).

[29] Bao T., Mezemir Damtie M., Hosseinzadeh A., Wei W., Jin J., Phong Vo H.N.; Ye J.S.; Liu Y., Wang X.F., Yu Z.M., Chen Z.J., Wu K., Frost R.L., Ni B.J., Bentonite-Supported Nano Zero-Valent Iron Composite as a Green Catalyst for Bisphenol a Degradation: Preparation, Performance, and Mechanism of Action, *Journal of Environmental Management*, **260**:110105 (2020).

[30] Li Chen X., Li F., Jie Xie X., Li Z., Chen L., Nanoscale Zero-Valent Iron and Chitosan Functionalized Eichhornia Crassipes Biochar for Efficient Hexavalent Chromium Removal, *International Journal of Environmental Research and Public Health*, **16**: 3046 (2019).

[31] Liu F., Yang J., Zuo J., Ma D., Gan L., Xie B., Wang P., Yang B., Graphene-Supported Nanoscale Zero-Valent Iron: Removal of Phosphorus from Aqueous Solution and Mechanistic Study, *Journal of Environmental Sciences*, **26**: 1751-1762 (2014).

[32] Mohan Kurmarayuni C., Kurapati S., Akhil S., Chandu B., Krishna Khandapu B., Koya P., Bollikolla H., Synthesis of Multifunctional Graphene Exhibiting Excellent Sonochemical Dye Removal Activity, Green and Regioselective Reduction of Cinnamaldehyde, *Materials Letters.*, **263**: 127224 (2020).

[33] Chen H., Cao Y., Wei E., Gong T., Xian Q., Facile Synthesis of Graphene Nano Zero-Valent Iron Composites and their Efficient Removal of Trichloronitromethane from Drinking Water, *Chemosphere*, **146**: 32-39 (2016).

[34] Xing M., Wang J., Nanoscaled Zero Valent Iron/Graphene Composite as an Efficient Adsorbent for Co(II) Removal from Aqueous Solution, *Journal of Colloid and Interface Science*, **474**: 119-128 (2016).

[35] Xing M., Xu L., Wang J., Mechanism of Co(II) Adsorption by Zero Valent Iron/Graphene Nanocomposite, *Journal of Hazardous Materials*, **301**: 286-296 (2016).

[36] Adel Niaei H., Rostamizadeh M., Adsorption of Metformin from an Aqueous Solution by Fe-ZSM-5 Nano-Adsorbent: Isotherm, Kinetic and Thermodynamic Studies, *The Journal of Chemical Thermodynamics*, **142**:106003 (2020).

[37] Li G., Xu Q., Jin X., Li R., Dharmarajan R., Chen Z., Enhanced Adsorption and Fenton Oxidation of 2,4-Dichlorophenol in Aqueous Solution Using Organobentonite Supported nZVI, *Separation and Purification Technology*, **197**: 401-406 (2018).

[38] Li L., Wang R., Xing X., Qu W., Chen Sh., Zhang Y., Preparation of Porous Semi-IPN Temperaturesensitive Hydrogel-Supported nZVI and its Application in the Reduction of Nitrophenol, *Journal of Environmental Sciences*, **82**: 93-102 (2019).

[39] Farinella N.V., Matos G.D., Arruda M.A.Z., Grape Bagasse as a Potential Biosorbent of Metals in Effluent Treatments, *Bioresource Technology*, **98**: 1940-1946 (2007).

[40] Gu M., Sui Q., Farooq U., Zhang X., Qiu Z., Lyu S., Enhanced Degradation of Trichloroethylene in Oxidative Environment by nZVI/PDA Functionalized rGO Catalyst, *Journal of Hazardous Materials*, **359**: 157-165 (2018).

[41] Alam Khan T., Dahiya S., Ahmad Khan E., Removal of Direct Red 81 from Aqueous Solution by Adsorption onto Magnesium Oxide-Coated Kaolinite: Isotherm, Dynamics and Thermodynamic Studies, *Environmental Progress & Sustainable Energy*, **36**: 45-58 (2017).

[42] Sabouri M.R., Sohrabi M.R., Zeraatkar Moghaddam A., A Novel and Efficient Dyes Degradation Using Bentonite Supported Zero- Valent Iron- Based Nanocomposites, *Chemistryselect*, **5**: 369 (2020).

[43] Veloso C.H., Filippov L.O., Filippova I.V., Ouvrard S., Araujo A.C., Adsorption of Polymers onto Iron Oxides: Equilibrium Isotherms, *Journal of Materials Research and Technology*, **9**: 779-788 (2020).

[44] Mudzielwana, R., Wilson, Gitari, M., & Ndungu, P., Performance Evaluation of Surfactant Modified Kaolin Clay in As(III) and As(V) Adsorption from Groundwater: Adsorption Kinetics, Isotherms and Thermodynamics, *Heliyon*, **5**: e02756 (2019).

[45] Mondal S., Majumder S.K., Honeycomb-Like Porous Activated Carbon for Efficient Copper (II) Adsorption Synthesized from Natural Source: Kinetic Study and Equilibrium Isotherm Analysis, *Journal of Environmental Chemical Engineering*, **7**: 103236 (2019).

[46] Saeed M., Munir M., Nafees M., Ahmad Shah S.S., Ullah H., Waseem A., Synthesis, Characterization and Applications of Silylation Based Grafted Bentonites for the Removal of Sudan Dyes: Isothermal, Kinetic and Thermodynamic Studies, *Microporous and Mesoporous Materials*, **291**: 109697 (2020).

[47] Kumari S., Ahmad Khan A., Chowdhury A., Bhakta A.K., Mekhalif Z., Hussain S., Efficient and Highly Selective Adsorption of Cationic Dyes and Removal of Ciprofloxacin Antibiotic by Surface Modified Nickel Sulfide Nanomaterials: Kinetics, Isotherm and Adsorption Mechanism, *Colloids and Surfaces A: Physicochemical and Engineering Aspects*, **586**: 124264 (2020).

[48] Kaur S., Jindal R., Synthesis of Interpenetrating Network Hydrogel from (gum copal alcoholscollagen)- co-poly (acrylamide) and Acrylic Acid: Isotherms and Kinetics Study for Removal of Methylene Blue Dye from Aqueous Solution, *Materials Chemistry and Physics*, **220**: 75-86 (2018).

[49] Naushad M., Abdullah Alqadami A., Abdullah AlOthman Z., Abdullah AlOthman Z., Hotan Alsohaimi I., Saad Algamdi M., Adsorption Kinetics, Isotherm and Reusability Studies for the Removal of Cationic Dye from Aqueous Medium Using Arginine Modified Activated Carbon, *Journal of Molecular Liquids*, **293**: 111442 (2019).

[50] Abdel-Mohsen A.M., Jancar J., Kalina L., Hassan A.F., Comparative Study of Chitosan and Silk Fibroin Staple Microfibers on Removal of Chromium (VI): Fabrication, Kinetics and Thermodynamic Studies, *Carbohydrate Polymers*, **234**: 115861 (2020).

[51] Amir Hossein M., Behzad H., Removal of Reactive Red 120 and Direct Red 81 Dyes from Aqueous Solutions by Pumice, *Research Journal of Chemistry and Environment*, **16**: 62-68 (2012).

[52] Dehghani M., Ansari Shiri M., Shahsavani S., Shamsedini N., Nozari M., Removal of Direct Red 81 Dye from Aqueous Solution Using Neutral Soil Containing Copper, *Desalination and Water Treatment*, **86**: 213-220 (2017).

[53] Khan T.A., Dahiya S., Ali I., Removal of Direct Red 81 Dye from Aqueous Solution by Native and Citric Acid Modified Bamboo Sawdust-Kinetic Study and Equilibrium Isotherm Analyss, *Gazi University Journal of Science*, **25**: 59-87 (2012).